Rock glaciers in the Central Eastern Alps – How permafrost degradation can cause acid rock drainage, mobilization of toxic elements and formation of basaluminite

Author(s):
Wanner, Christoph; Moradi, Hoda; Ingold, Philipp; Cardenas Bocanegra, Miguel A.; Mercurio, Romano; Furrer, Gerhard

Publication date:
2023-08

Permanent link:
https://doi.org/10.3929/ethz-b-000620434

Originally published in:
Global and Planetary Change 227, https://doi.org/10.1016/j.gloplacha.2023.104180

Global and Planetary Change 227 (2023) 104180

Contents lists available at ScienceDirect

Global and Planetary Change

journal homepage: www.elsevier.com/locate/gloplacha

Rock glaciers in the Central Eastern Alps – How permafrost degradation can cause acid rock drainage, mobilization of toxic elements and formation of basaluminite

Christoph Wanner [a,*], Hoda Moradi [a], Philipp Ingold [a], Miguel A. Cardenas Bocanegra [a], Romano Mercurio [a], Gerhard Furrer [b]

[a] Rock-Water Interaction Group, Institute of Geological Sciences, University of Bern, Baltzerstrasse 3, CH-3012 Bern, Switzerland
[b] Institute of Biogeochemistry & Pollutant Dynamics, ETH Zurich, 8092 Zurich, Switzerland

ARTICLE INFO

Editor: Liviu Matenco

Keywords:
Climate change
Pyrite weathering
Aluminum
Drinking water quality
Environmental hazard

ABSTRACT

Naturally occurring acid rock drainage (ARD) appears to be promoted in permafrost environments with pyrite-bearing host rocks. However, it is poorly understood how the interaction between solid ice, meltwater and pyrite causes the formation of sulfuric acid and the subsequent mobilization of toxic elements. To elucidate the governing processes and to assess the general hazard of ARD in permafrost areas in the context of global warming, we present chemical water analyses for six high-alpine surface waters downstream of intact rock glaciers in the Central Eastern Alps. In addition, we provide a detailed chemical and structural characterization of nanocrystalline Al-hydroxysulfate precipitates forming along the streams and serving as a visual manifestation of ARD. Finally, we show results from column experiments, experimentally simulating the interaction between water and pyrite-bearing paragneisses. Studying ARD on both, the field and laboratory scales, demonstrated that under field-site conditions intact rock glaciers may act as highly efficient chemical reactors, resulting in high concentrations of toxic elements such as aluminum, nickel, manganese, and fluorine in the sampled high-alpine streams. The most likely reason for the strong mobilization of these elements is their temporal storage and enrichment in the frozen rock glacier core, leading to a quick and focused export in summer when ice melt production rates are high. The analyses of the Al-hydroxysulfate precipitates confirmed the presence of basaluminite ($Al_4(OH)_{10}(SO_4)$ x 3 H_2O), controlling the solubility of aluminum. Geochemical modeling allowed to quantify the inverse behavior of the basaluminite solubility with temperature, resulting in a field-derived standard reaction enthalpy ($\Delta_r H°$) of −580 kJ mol $^{-1}$. This value can now be used to determine the solubility of aluminum also at temperatures relevant for permafrost settings (0–5 °C). Aerial photographs of the study sites suggest a strong intensification of ARD in the Central Eastern Alps over the past 20 years, and that the flux of toxic elements mobilized from intact rock glaciers may further increase in the future. Owing to the high abundance of pyrite-bearing rocks, the same may apply to areas downstream of intact rock glaciers worldwide. In conclusion, the water quality downstream of intact rock glaciers with pyrite-bearing rocks must be carefully monitored to assess the future environmental hazard.

1. Introduction

In many parts of the world, acid rock drainage (ARD) is a serious environmental problem (Blowes et al., 2005; Tuffnell, 2017). First of all, the problem occurs in the vicinity of sulfide or coal mines where the oxidation of pyrite-rich tailings leads to the formation of sulfuric acid and the subsequent mobilization of toxic elements (Nordstrom and Alpers, 1999; Bigham and Nordstrom, 2000). Such anthropogenically induced ARD is commonly described as acid mine drainage (AMD). In addition, ARD occurs naturally in watersheds with sulfide-rich bedrock without any mining activities. A typical setting for natural ARD appears to be downstream of glaciers or ice-rich permafrost (e.g. rock glaciers) in mountainous or high-latitude catchments. Examples include high-alpine, periglacial environments of the Central Eastern Alps (Ilyashuk et al., 2014, 2018), the Pyrenees (Zarroca et al., 2021), and the Rocky Mountains (Mast et al., 2011; Todd et al., 2012), as well as the foreland

* Corresponding author.
E-mail address: christoph.wanner@unibe.ch (C. Wanner).

https://doi.org/10.1016/j.gloplacha.2023.104180
Received 24 January 2023; Received in revised form 29 May 2023; Accepted 15 June 2023
Available online 17 June 2023

of glaciers such as in Peru (Fortner et al., 2011) or the shoreline of King George Island in Antarctica (Dold et al., 2013). These examples suggest that ARD may become more frequent as climate change progressively thaws glaciers and permafrost (e.g. Haeberli and Beniston, 1998; Pogliotti et al., 2015; PERMOS, 2020), exposing more sulfide-rich bedrock to aerobic waters. This hypothesis is supported by a long-term monitoring of the Upper Snake River in Colorado, USA, demonstrating that sulfate and Zn concentrations, both products of ARD, have continuously increased since the 1970ies (Todd et al., 2012), and the strong intensification of natural ARD in the Noguera de Vallferrera catchment in the Pyrenees, Spain, documented since 1945 using aerial photographs (Zarroca et al., 2021). Similarly, a six-fold increase in sulfate concentrations has been reported for a high alpine lake in the South Tyrol area in Northern Italy between 1985 and 2005 (Thies et al., 2007), which – according to a later study – is also affected by ARD (Ilyashuk et al., 2014).

The pH values of the effluents in AMD areas typically range between 2 and 4 (Bigham and Nordstrom, 2000). Together with high concentrations of iron and sulfate, this leads to the precipitation of secondary Fe-hydroxysulfates causing the rust-colored streamwater typical for such sites. In contrast, the pH of the effluents in naturally occurring ARD areas typically range between 4 and 6, and the dissolved iron concentration is relatively low. Together with elevated concentrations of sulfate and aluminum, this leads to the precipitation of white-colored, secondary Al-hydroxysulfates such as basaluminite (Adams and Rawajfih, 1977; Nordstrom et al., 1984; Ball and Nordstrom, 1989; Bigham and Nordstrom, 2000; Jones et al., 2011; Sánchez-España et al., 2011; Carrero et al., 2015; Caraballo et al., 2019). The formation of these precipitates is characteristic for ARD sites and it controls the mobility of aluminum and other toxic elements.

In the Central Eastern Alps, the occurrence of XRD-amorphous, nanocrystalline basaluminite has been described in Eastern Switzerland along a high-alpine stream called “Ova Lavirun” (Wanner et al., 2018), originating from an ice-rich permafrost area (Kenner et al., 2019) that can be classified as intact rock glacier. The onset of basaluminite precipitation occurs at a distinct location where the acidic stream (pH ~ 4.5) is neutralized to pH 5.5 by a merging pH-neutral tributary. Beside its acidic pH, Ova Lavirun is characterized by elevated concentrations of Al, Ni, Mn, and F^- ([Al] >20 mg/L; [Ni] >1 mg/L; [Mn] > 5 mg/L; [F^-] > 5 mg/L), strongly exceeding the Swiss drinking water limit at the stream origin where the temperature is below 1 °C ($[Al]_{limit}$: 0.2 mg/L; $[Ni]_{limit}$: 0.02 mg/L; $[Mn]_{limit}$: 0.05 mg/L; $[F^-]_{limit}$: 1.5 mg/L). Similar concentrations of Al and Ni were reported for the Lazaunbach stream in Northern Italy, which also originates from a rock glacier spring. As a consequence, a local high-alpine farm had to look for alternative, uncontaminated drinking water resources (Mair et al., 2015). These two examples demonstrate the potential hazard of naturally occurring ARD for surface water quality on the regional scale of the Central Eastern Alps and in similar high-alpine settings worldwide.

While the geographical link between natural ARD and permafrost areas is well documented, it remains unclear how the interaction between solid ice, meltwater and pyrite-bearing rocks promotes the formation of sulfuric acid and the subsequent mobilization of toxic elements (Colombo et al., 2018; Brighenti et al., 2019). Moreover, thermodynamic data for basaluminite are restricted to 25 °C (Singh and Brydon, 1969; Adams and Rawajfih, 1977; Sánchez-España et al., 2011; Lozano et al., 2018). Since the temperature dependence of the log(K) value of basaluminte is likely strong (Wanner et al., 2018), this precludes to accurately predict the mobility of aluminum in mountainous or high-latitude watersheds at temperatures close to 0 °C.

After publication of the Ova Lavirun case study in Eastern Switzerland (Wanner et al., 2018), interested readers reported eight additional streams in the Central Eastern Alps, where white-colored streambeds are observed as well. For this contribution, we present chemical water analyses for six of the reported streams and a detailed chemical and structural characterization of the corresponding precipitates. In addition, we show results from column experiments, experimentally simulating the interaction between water and pyrite-bearing paragneisses frequently occurring in the Central Eastern Alps. Studying ARD on both the field and laboratory scales provides novel insights into the fundamental processes, causing the mobilization of aluminum and other toxic elements from permafrost areas. Moreover, it improves our understanding of the processes controlling the precipitation and stability of Al-hydroxysulfates, which serve as an important natural sink for aluminum and other toxic elements (Carrero et al., 2017b; Wanner et al., 2018). Both type of information is key to assess the future hazard caused by ARD in permafrost areas worldwide in the context of global warming.

2. Site description

The high-alpine streams with white-colored streambeds sampled in this study (Fig. S1, Electronic Appendix) are all located in similar geological units, which are part of the crystalline basement of the Austroalpine nappes (Fig. 1). The same applies to previously reported white-colored streambeds such as along Ova Lavirun (Wanner et al., 2018), in the Kaunertal (Thies et al., 2017) and at Lake Rasass (Ilyashuk et al., 2014). The crystalline basement nappes of the Austroalpine nappes are free of carbonates and mainly consist of two general crystalline rock types: (i) polymetamorphic paragneisses and micashists originally deposited as clastic sediments and (ii) intrusive rocks outcropping as metagranites or orthogneisses today (Pfiffner, 2009). Strongly weathered paragneisses display a distinct rusty weathering colour (Fig. S1, Electronic Appendix), inherited from the oxidation of pyrite, enriched in many of these rocks (Peters, 2005).

The origins of the white-colored streams are generally located on north-east to north-west facing slopes above 2600 m a.s.l. (Fig. S2, Electronic Appendix) where permafrost is present in nearly all conditions (Boeckli et al., 2012). In addition, the occurrence of rock glaciers as a manifestation of ice-rich permafrost conditions is evident in the catchments of most of the reported streams (Fig. S3, Electronic Appendix). Rock glaciers are high-alpine, quaternary landforms consisting of debris of variable grain sizes. Within the top 0.5–5 m, they consist of a seasonally frozen, blocky layer known as the active layer that thaws each summer (Jones et al., 2018a). Below the active layer, there is the frozen core of the rock glacier where the pores of the debris are fully saturated with ice (Jones et al., 2019; and references therein). Rock glaciers are subject to internal deformation of the ice leading to a gravity-driven creep of these landforms. If all ice has molten, rock glaciers stop to creep and are classified as relict (Jones et al., 2018b, 2019). Owing to the high altitude above 2600 m a.s.l. and the low discharge temperature of the corresponding springs (see below), the rock glaciers present at the origin of the reported white-colored streams are all considered as intact (i.e. containing ice).

An additional similarity of the reported white-colored streams (Fig. 1) is that the onset of the white-colored stream segments occurs downstream of the actual stream origins. In contrast to the previously reported sites at Ova Lavirun (Wanner et al., 2018) and in the Kaunertal (Thies et al., 2017), however, the onsets of these segments are diffuse and not related to a single tributary.

3. Methods

3.1. Sampling of streamwater and white precipitates

Overall, 20 streamwater samples from six high-alpine streams with white-colored stream sections were collected between July 2019 and August 2021. For each site, at least one sample from the origin of the stream and one from the white-colored section was taken. All sampling locations are shown on maps of the individual systems provided in the Electronic Appendix (Fig. S2). The pH, electrical conductivity (EC), O_2 saturation, and sampling temperature were measured on-site using

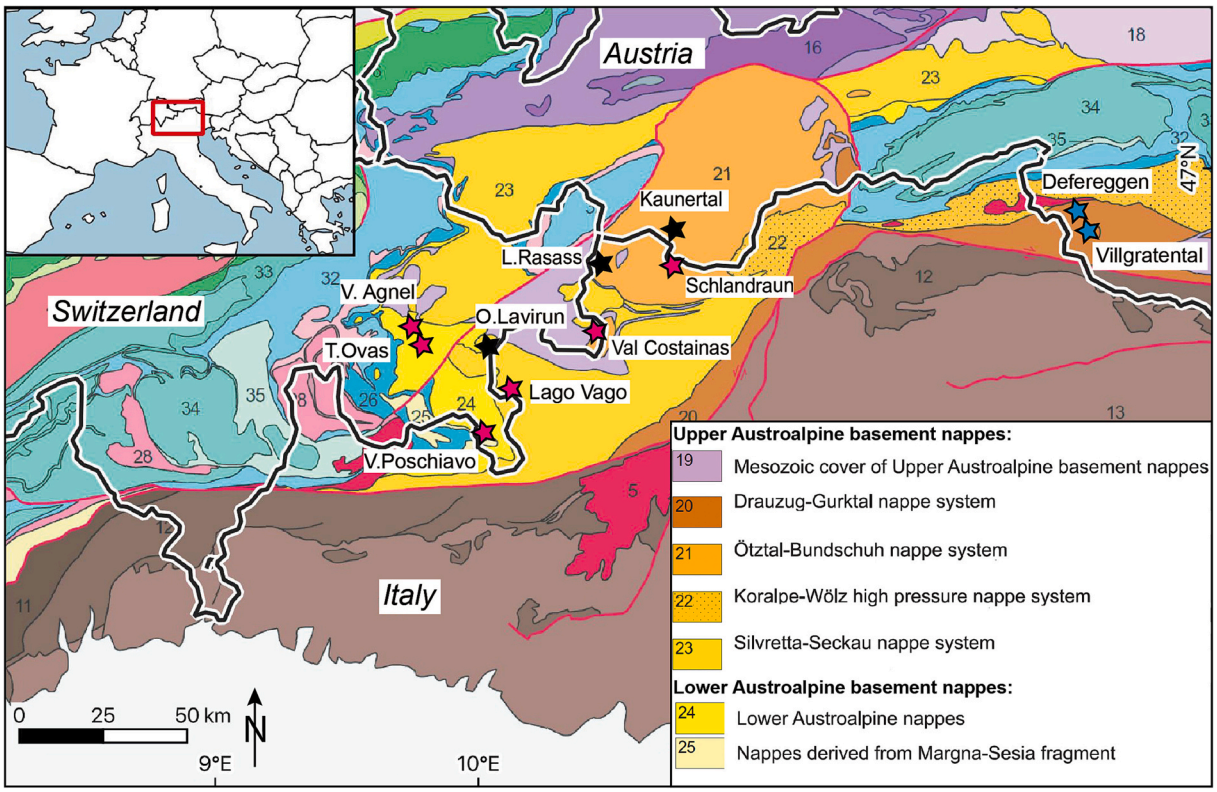

Fig. 1. Tectonic map of the Central Eastern Alps (modified from Schmid et al., 2004) and occurrences of white-colored streambeds shown as star symbols (red: newly reported streams sampled in this study; blue symbols: newly reported streams but no samples collected; black symbols: streams previously reported and characterized (Ilyashuk et al., 2014; Thies et al., 2017; Wanner et al., 2018)). The legend is only provided for the tectonic units hosting the white-colored streams, which are all part of the crystalline basement of the Austroalpine Nappes. A lithological description of the tectonic units is provided in the text. (For interpretation of the references to colour in this figure legend, the reader is referred to the web version of this article.)

Hamilton electrodes with Knick Portamess-913 field instruments. After sampling, two aliquots per sample were filtered at 0.2 μm and stored in polyethylene bottles. The aliquots for the analysis of major cations and trace elements were acidified to pH 3 by adding one drop of 65% HNO_3. Prior analysis, samples were stored at 4 °C. Precipitate samples from the white-colored stream segments were obtained by scratching from air-dried rock specimen collected along the different stream systems using a stainless-steel spatula.

3.2. Column experiments

To experimentally study acid rock drainage, three column experiments were conducted using paragneiss rock specimen collected from the Ova Lavirun reference site (Wanner et al., 2018) and the Lago Vago site studied in this study (Table 1). Running experiments with rock samples from different sites allows testing the sensitivity of acid rock drainage with respect to the mineralogical composition. The rock specimen from the two sites were chosen based on their strong contrast in sulfur concentration (Table 1).

To run the experiments, the rock specimen were crushed, milled and sieved for grain size fractions ≤0.25 mm, 0.25–2 mm, and > 2 mm. Subsequently, they were packed into ca. 25 cm long acrylic columns with a diameter of 2.5 cm. Assuming that the reactivity of the crushed rock increases with decreasing grain size but allowing for sufficient porosity and permeability to flush the columns, the fraction 0.25–2 mm was used to fill one column for each site. To assess the sensitivity of the experimental results with respect to the grain size fraction, the third column was filled with a mix of the ≤0.25 mm and 0.25–2 mm fractions of the crushed Ova Lavirun rock specimen.

Initially, the filled columns were flushed with about three pore volumes of deionized water (< 0.6 μS/cm) using a peristaltic pump at maximal flow rate (5 mL/min) to remove initially desorbing solutes. Afterwards, the pump was stopped until sampling took place after a certain time of no flow conditions (i.e. batch mode). Sampling was conducted by restarting the pump at a low flow rate (<1 mL/min). The first 5 mL of the effluent were discarded before the next 10 mL were collected, eventually. All effluent samples were preserved using the same techniques (filtration and acidification) as described above for the

Table 1
Key physical and chemical properties of the crushed rock used to run the column experiments.

Experiment	Sample origin (Fig. 1)	Grain size fraction	Column length (cm)	Pore volume (mL)	Porosity	[1]SiO_2 (wt%)	[1]Al_2O_3 (wt%)	[1]SO_3 (wt%)
Column 1	Lago Vago	0.25–2 mm	18.5	18.5	0.32	59.7	18.6	1.066
Column 2	Ova Lavirun	0.25–2 mm	19.7	28.7	0.46	51.8	25.8	0.219
Column 3	Ova Lavirun	1/3 (<0.25 mm) + 2/3 (0.25–2 mm)	21.2	28.6	0.43	48.4	26.9	0.245

[1] Concentration in crushed rock material. Full XRF analyses are provided in the Electronic Appendix (Table S1).

streamwater samples. Owing to the small sample volumes, only the pH was measured during sampling. After sampling, the columns were again flushed with at least three pore volumes of deionized water to restart the experiment with pure deionized water and a higher residence time. For all three columns, samples were taken after residence times of 1, 2, 4, 8 and 16 weeks.

3.3. Analytical methods

3.3.1. Water analyses

Streamwater and effluent samples from the column experiments were analyzed at the University of Bern. Concentrations of Na^+, NH_4^+, K+, Ca^{2+}, Mg^{2+}, F^-, Cl^-, Br^-, NO_3^- and SO_4^{2-} were measured by ion chromatography (Metrohm 850 Professional). For cations, a detection limit of 0.1 mg/L was reached, while the detection limit for anions was 0.016 mg/L. Concentrations of Al, Co, Cu, Fe, Pb, Mn, Ni, Si, Sr and Zn were determined by inductively coupled plasma optical emission spectroscopy (ICP-OES) using a Varian 720-ES. The detection limits was 50 µg/L for Al, Cu, Pb and Si, and 5 µg/L for Co, Fe, Mn, Ni, Sr and Zn. The concentration of As was determined by atomic adsorption spectroscopy (AAS) using a ContrA 700 (Analytik Jena) with a detection limit of 4 µg/L. The analytical error of all these measurements was ±5%. Total inorganic carbon concentrations were determined using a Multi N/C 20100S TIC/TOC analyzer (Analytic Jena) with a detection limit of 0.1 mg/L and an analytical uncertainty of ±5%.

3.3.2. Analyses of white precipitates

Following Carrero et al. (2017b), the chemical composition of one precipitate sample per sampled stream system was analyzed by total digestion of 0.05 g per sample in 5 mL of 65% HNO_3. Subsequently concentrations of Al, Ca, Cu, Fe, K, Mg, Mn, Na, S and Si were determined by ICP-OES with detection limits of 0.5 mg/L for S, 50 µg/L for Al and Fe, 10 µg/L for Ca, Cu and Si, and 5 µg/L for Mg, Mn, K and Na. Owing to the prevailing oxidizing conditions in the streamwaters (Wanner et al., 2018), the measured concentrations of S were converted to SO_4. As for the water samples, AAS was used to determine the concentration of As. The analytical error of all these measurements was ±5%.

The structure of the precipitates was analyzed by X-ray diffraction (XRD) and Fourier-transformed infrared spectroscopy (FTIR) at the University of Bern. For FTIR, 11 mg air-dried samples were ground together with 500 mg of dried KBr (105 °C). Spectra were recorded by a Bruker Vertex 70 spectrometer over a range of 500–4000 cm^{-1} with 2 cm^{-1} resolution and 100 scans. For XRD, ca. 1 mg of air-dried samples were put on a silica plate. Subsequently, XRD patters were recorded using a Malvern Panalytical Empyrean diffractometer (Cu-Kα X-ray source: 1.5401 Å) over a 2θ range of 5–75° with a step size of 0.02°, and an acquisition rate and time of 0.08° s^{-1} and 25 s per step, respectively.

3.3.3. Chemical analysis of column experiment material

The chemical composition of the crushed rock samples used for the column experiments was determined by X-Ray fluorescence spectroscopy (XRF). To do so, pressed powder pellets obtained by adding Hoechstwax and pressing the corresponding mixtures at 15 t during 4 min, were measured with a Wavelength-Dispersive X-Ray fluorescence (WD-XRF) spectrometer (PANalytical Zetium) equipped with a Rh-anode X-Ray tube at the University of Fribourg, Switzerland. Subsequently, major and trace elements concentrations were semi-quantitatively determined using the standardless calibration provided by the OMNIAN software (Malvern Panalytical). The detection limit and measurement uncertainty were estimated to 30 µg/g and ± 5%, respectively.

The composition of opaque minerals in the rock sample from Val Lavirun was semi-quantitatively determined by preparing thin sections followed by scanning electron microscopy (SEM) in combination with standardless energy dispersive X-ray spectroscopy (EDX) at the University of Bern using a Zeiss EVO50 SEM. The detection limit for the EDX measurements and the corresponding measurement uncertainty were estimated to 0.1 wt% and ± 5%, respectively.

4. Results

4.1. Streamwater samples

The chemical composition of streamwater samples collected from the six high-alpine streams in the Central Eastern Alps is listed in Table 2 and in the Electronic Appendix (Table S2). Concentrations of major cations and anions are plotted on classical Schoeller and Piper diagrams (Fig. 2). According to the water classification of Jäckli (1970), all samples either correspond to the Mg-Ca-SO_4 or the Ca-Mg-SO_4 water type. The similarity of the streamwater samples is further manifested by similar patterns in the Schoeller diagram and the fact that they appear on the same region on the Piper diagram subplots. With very few exceptions, the concentrations of Al, Ni, Mn, and F are above detection and, in most cases, strongly exceed the corresponding drinking water limits. Likewise, also the concentration of Co was above detection in most of the stream origins (Table S2, Electronic Appendix). In addition, the sampling temperature at the origin of the streams is in most cases below 2 °C and thus close to the melting point of ice. Finally, all samples are close to saturation with dissolved oxygen and show dissolved iron concentration below detection.

The main differences in the chemical composition of the streamwater samples relate to variations of (i) the Ca and Mg ratio, (ii) the total dissolved solid (TDS) concentration as well as concentrations of individual solutes, and (iii) the pH ranging from 4.5 to 6.9. On the one hand, these differences are a manifestation of the different streams, from which samples were taken. For instance, the pH and TDS concentrations at the stream origins range from 4.5 to 5.8 and 146 to 1677 mg/L, respectively. On the other hand, however, there is a clear trend of decreasing solute concentrations as well as increasing pH and temperatures with increasing distance from the stream origins.

4.2. White precipitates

4.2.1. Structural characterization

The XRD pattern and FTIR spectra of the precipitate samples collected from the six streams are shown in Fig. 3 in comparison to a basaluminite sample collected from the Ova Lavirun reference system and previously described in detail (Wanner et al., 2018). Beside small quartz and clay peaks likely representing minor contamination inherited from scratching the precipitates off the rock specimen, none of the recorded XRD patterns show any distinct peaks. This demonstrates the XRD amorphous structure of the collected precipitates. Despite the lack of strong peaks, the XRD patterns display rather strong similarities to that of the basaluminite sample collected from Ova Lavirun (Wanner et al., 2018). Likewise, in the FTIR spectra all six precipitates show very strong similarities among each other as well as with the reference basaluminite sample from Ova Lavirun (Wanner et al., 2018).

4.2.2. Chemical characterization

The chemical composition of precipitates collected from the six streams is shown in Table 3. All samples are dominated by H_2O + OH, and aluminum at similar concentrations, comparing well with those of the reference basaluminite sample from Ova Lavirun (Wanner et al., 2018). In contrast, the sulfate concentrations show notable differences. This is reflected in the Al/SO_4 ratio ranging from 4.5 to 6.8. Nevertheless, the ratios are close to those of basaluminite with an ideal stoichiometry of $Al_4OH_{10}(SO_4)$ x $(H_2O)_{3–5}$ (Al/SO_4 = 4.0) and the reference basaluminite sample from Ova Lavirun (Al/SO_4 = 5.1, Table 3). Together with the XRD and FTIR analyses (Fig. 3), this confirms the formation of nanocrystalline basaluminite along most of the sampled streams.

Table 2
Key parameters of streamwater samples collected from six high-alpine streams with whitened streambed sections between July 2019 and August 2021. Also listed are the ranges of these parameters in the column experiment effluent samples, as well as the Swiss drinking water limits for Al, Ni, Mn and F^-. The sampling dates and full chemical analyses of both the streamwater and the column effluent samples are provided in Tables S2 and S3 (Electronic Appendix). The sampling locations for the streamwater samples are provided on Fig. 1 and in the Electronic Appendix (Fig. S2, Table S2).

Sample	Site	Sample type	T (°C)	Altitude (m a.s.l.)	pH	TDS (mg/L)	Water type	Al (mg/L)	Ni (mg/L)	Mn (mg/L)	F^- (mg/L)
AP1	Val Costainas	Stream origin	0.7	2660	4.98	1677	Mg-Ca-SO_4	14.8	0.84	2.29	14.96
AP5	Val Costainas	White-colored segment	4.9	2530	5.56	800	Mg-Ca-SO_4	3.6	0.51	0.90	4.92
AP8	Val Costainas	White-colored segment	7.5	2405	5.74	540	Mg-Ca-SO_4	2.1	0.34	0.57	3.03
AP9	Val Costainas	White-colored segment	5.0	2305	6.20	445	Mg-Ca-SO_4	1.4	0.27	0.40	2.29
AP10	Val Costainas	White-colored segment	10.6	1890	6.21	345	Mg-Ca-SO_4	0.2	0.20	0.28	1.59
PC1	Val Poschiavo	Stream origin	5.1	2645	4.50	395	Ca-Mg-SO_4	9.6	0.51	2.04	1.64
PC4	Val Poschiavo	White-colored segment	11.6	2560	5.15	86	Ca-Mg-SO_4	1.5	0.14	0.43	0.36
PC5	Val Poschiavo	White-colored segment	12.2	2540	5.17	81	Ca-Mg-SO_4	1.1	0.13	0.38	0.33
PC6	Val Poschiavo	White-colored segment	12.5	2500	5.53	74	Ca-Mg-SO_4	0.7	0.11	0.33	0.30
TO1	Traunter Ovas	Stream origin	3.5	2715	4.70	573	Ca-Mg-SO_4	21.7	0.08	6.00	5.27
TO2	Traunter Ovas	White-colored segment	7.5	2710	5.15	496	Ca-Mg-SO_4	10.0	0.05	2.82	6.21
TO3	Traunter Ovas	White-colored segment	8.8	2660	5.00	347	Ca-Mg-SO_4	8.6	0.04	2.31	2.97
TO4	Traunter Ovas	White-colored segment	9.8	2650	5.08	322	Ca-Mg-SO_4	5.6	0.03	1.80	2.51
VA4	Vadret Agnel	Stream origin	1.4	2795	4.46	146	Ca-Mg-SO_4	4.5	<0.05	0.64	0.08
VA5	Vadret Agnel	White-colored segment	5.3	2770	5.18	143	Ca-Mg-SO_4	3.1	<0.05	0.46	0.09
VA6	Vadret Agnel	White-colored segment	8.5	2760	6.60	123	Ca-Mg-SO_4	0.3	<0.05	<0.05	0.64
LV7B	Lago Vago	Stream origin	1.9	2687	4.89	388	Ca-Mg-SO_4	4.5	0.16	0.96	0.06
LV8	Lago Vago	White-colored segment	9.1	2680	5.30	244	Ca-Mg-SO_4	1.5	0.10	0.49	0.06
ST1	Schlandraun	Stream origin	1.9	2770	5.10	853	Ca-Mg-SO_4	5.3	0.69	1.14	1.86
ST3	Schlandraun	White-colored segment	7.7	2685	5.23	502	Ca-Mg-SO_4	3.5	0.36	0.61	0.82
Column experiment effluent samples					5.3–6.7	44–242	Variable	≤0.14	≤0.03	0.05–0.27	0.02–0.07
Swiss drinking water limit[1]								0.2	0.02	0.05	1.50

[1] See https://www.fedlex.admin.ch/eli/cc/2017/153/de

The precipitate from Lago Vago shows an As concentration of 1356 μg/g, which is even higher than that of the Ova Lavirun reference basaluminite. Even though all other samples show As concentrations at or below the detection limit, this confirms that basaluminite may operate as a highly efficient sink for arsenic.

4.3. Column experiments

4.3.1. Chemical characterization of solid material

The full chemical composition of the crushed rocks used to run the column experiments is provided in Table 1 as well as in the Electronic Appendix (Table S1). With SiO_2 concentrations ranging between 48 and 60 wt% and elevated concentrations of Al (29–27 wt% Al_2O_3) and Fe (8–12 wt% Fe_2O_3), the column experiment materials compare well with other paragneisses of the Central Eastern Alps (e.g., Siegesmund et al., 2018).

Almost all of the opaque minerals occurring in the thin sections of the Ova Lavirun rock specimen were identified as pyrite (Fig. S4, Electronic Appendix). While most of the analyzed pyrite crystals did not show any detectable trace elements, a few grains yielded Ni, Zn, and Co concentrations up to 4.3, 5.3 and 2.4 wt% (Table S4, Electronic Appendix).

4.3.2. Effluent water samples

The full chemical compositions of column effluent samples are listed in the Electronic Appendix (Table S3), while a comparison with the streamwater samples is provided in Table 2. In analogy to the streamwater samples, either Ca or Mg is the major cation, while SO_4 is always the dominating anion. The similarity to the streamwater samples is manifested by comparable patterns in the Schoeller diagram and the fact that the column effluent samples plot on similar regions on the Piper diagram subplots (Fig. 2), although they generally show higher relative concentrations of Na and K. Likewise, with a minimum value of 5.3, the pH values of the column effluents compare well with those of the sampled streams. Finally, all toxic elements showing high concentrations in the streamwater samples (Al, Ni, Mn, F) were detected at least once in the column effluents. The concentrations of major and trace solutes, however, are up to two orders of magnitude lower than those measured in the streamwater samples.

Interestingly, the concentrations of major solutes such as SO_4 showed a contrasting behavior as a function of the column residence time (Fig. 4). While the SO_4 concentration in the effluents of Column 1 and 3 decreased with increasing residence time, the concentration in the effluent of Column 2 increased by a factor of 1.8. In addition, the maximum SO_4 concentration in the effluent of Column 1 (crushed rock from Lago Vago) was much higher than those in the effluent of Column 2 and Column 3 (crushed rock from Ova Lavirun) showing very similar values. The ratio between the maximum concentrations was about 6.

5. Discussion

5.1. Mobilization of aluminum and other toxic elements in intact rock glaciers

5.1.1. Pyrite oxidation as main weathering agent

The similarity of the streamwater and column experiment effluent samples with respect to both, major and toxic element concentrations confirms that the acidic conditions and high solute concentrations of the sampled high-alpine streams are solely inherited from water-rock interaction processes. For all samples, the sum of the equivalents of major cations (Na^+, K^+, Ca^{2+}, Mg^{2+}, Al^{3+}) plot very close to a 1:1 correlation with respect to the corresponding SO_4^{2-} concentrations (Fig. 5). This demonstrates that SO_4^{2-} fully charge balances all the cations in the samples, providing strong evidence that sulfuric acid (H_2SO_4) is the main weathering agent causing the dissolution of the pyrite-bearing paragneiss host rocks typical for the Austroalpine basement nappes. Sulfuric acid is inherited from the oxidation of pyrite by dissolved

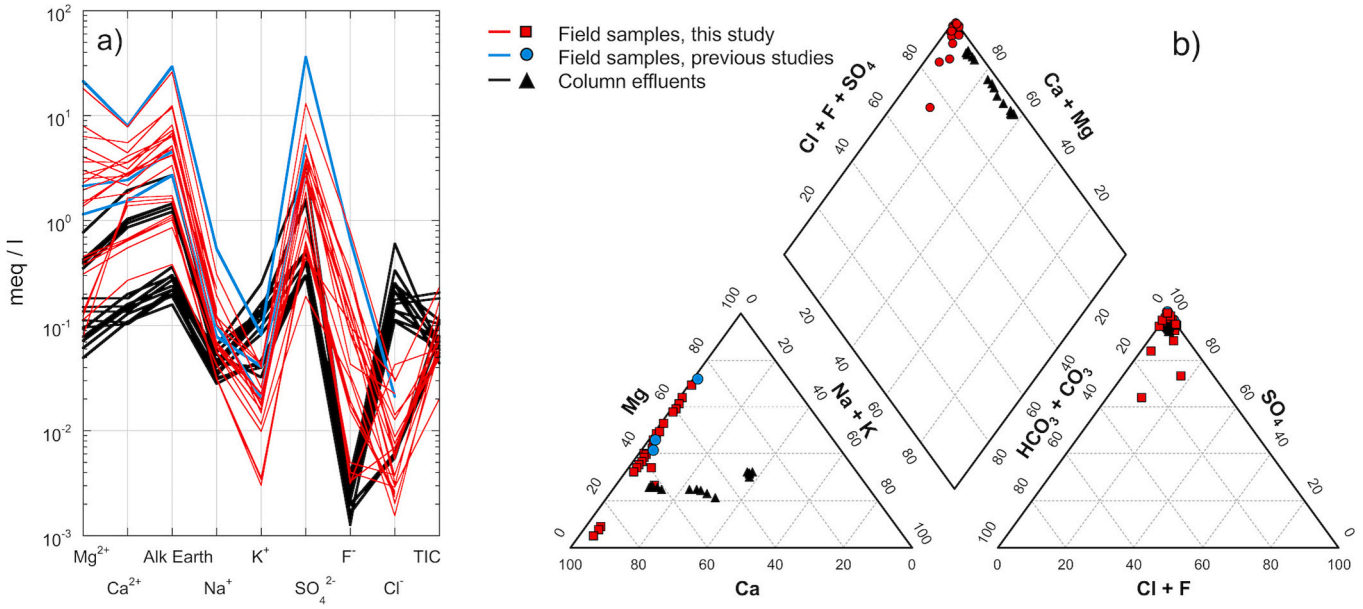

Fig. 2. Schoeller (a) and Piper (b) diagrams for streamwater samples collected between July 2019 and August 2021 along six high-alpine streams of the Central Eastern Alps (red lines and symbols). Previously published samples from similar settings in the Central Eastern Alps such as Ova Lavirun (Wanner et al., 2018), the outlet of lake Rasass (Ilyashuk et al., 2018), and the outlet of the Krummgampen rock glacier in the Kaunertal (Thies et al., 2013) are plotted as well (blue lines and symbols). In addition, the black lines and symbols refer to effluent samples from the column experiments. (For interpretation of the references to colour in this figure legend, the reader is referred to the web version of this article.)

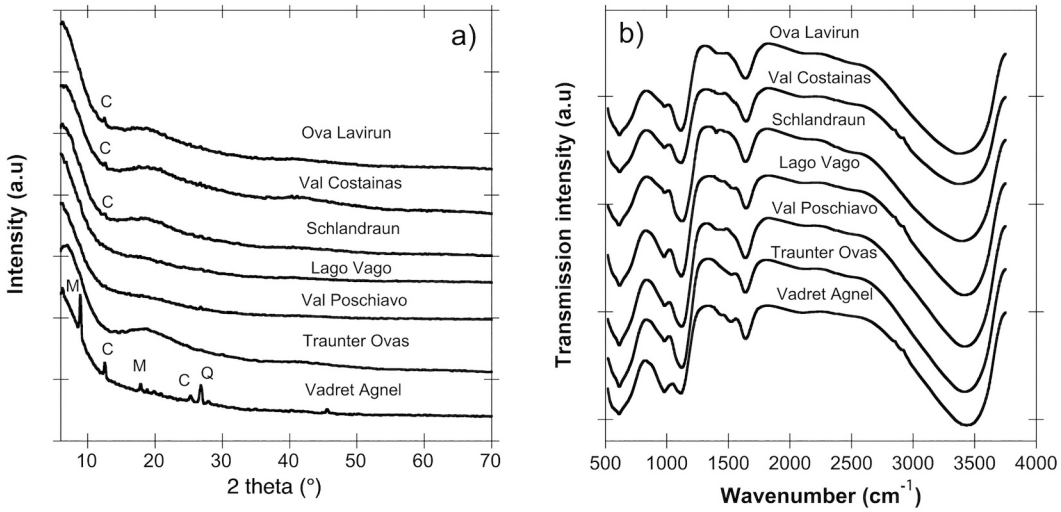

Fig. 3. XRD patterns (a) and FTIR spectra (b) of white precipitate samples collected from six high-alpine streams in the Central Eastern Alps (Fig. 1) as well as of a reference basaluminite sample from the Ova Lavirun system (Wanner et al., 2018). Small peaks in the XRD patterns represent minor contamination likely inherited from scratching the precipitates off the rock specimen. M: Muscovite, biotite, or illite. C: Chlorite. Q: Quartz.

oxygen leading to acidic condition as well as the precipitation of Fe-hydroxides ($Fe(OH)_{3(s)}$), manifested by the rusty weathering colour of the local host rocks (Fig. S1, Electronic Appendix):

$$4\,FeS_2 + 15\,O_2 + 14\,H_2O \rightarrow 4\,Fe(OH)_{3(s)} + 8\,H_2SO_4 \quad (1)$$

In the absence of buffering carbonates, the low pH accelerates the dissolution of the Al-rich paragneisses, leading to a typical ARD scenario with high solute concentrations at the origin of the streams including those of Al and other toxic elements (Table 2). While elevated concentrations of Ni, Zn, and Co are clearly inherited from the enrichment of these elements in pyrite (Table S4, Electronic Appendix), the source for the high concentrations of F^- and Mn remains unclear. Possible candidates include fluorite or apatite for F^-, as well as Mn-oxides for Mn.

The differences in the Ca/Mg ratio in the sampled streams and the higher relative contribution of Na and K in some of the column experiment effluent samples (Fig. 2) are likely inherited from a variation of the host rock mineralogy with respect to the dominating Ca-, Mg-, Na-, and K-silicates. Thus, the governing dissolution reactions slightly vary from site to site. The dissolution of silicate minerals acts as pH buffer as demonstrated by the dissolution reaction of chlorite, which is one of the most abundant Mg-silicates in the paragneisses of the Austroalpine basement nappes:

$$Mg_5Al(AlSi_3O_{10})(OH)_8 + 8\,H_2SO_4 \rightarrow 5\,Mg^{2+} + 2\,Al^{3+} + 3\,SiO_2 + 12\,H_2O + 8\,SO_4^{2-} \quad (2)$$

Therefore, mineralogical variations result in minor shifts of the pH

Table 3
Chemical composition of white precipitate samples collected along six high-alpine streams in the Central Eastern Alps. The sampling locations are provided on Fig. 1 and in the Electronic Appendix (Fig. S2, Table S2).

	Unit	Val Costainas	Val Poschiavo	Traunter Ovas	Vadret Agnel	Lago Vago	Schlandraun	Val Lavirun[1]
Sample name	n.a	AP5	PC4	TO4	VA6	LV8	ST3	OL9
Streamwater pH	–	5.58	5.15	5.08	6.93	5.3	5.23	5.3
$H_2O + OH$	wt%	62.4	63.8	60.1	67.3	58.4	59.3	54.4
Al	wt%	24.4	21.8	22.5	20.1	23.8	21.7	26.7
SO_4	wt%	13.6	14.7	17.7	10.5	17.7	18.0	18.5
Si	wt%	0.71	0.54	0.37	0.7	2.6	0.007	0.2
Fe	wt%	0.19	0.07	0.03	0.3	0.60	0.1	0.09
Ca	wt%	0.07	0.13	0.03	0.7	1.0	0.01	0.01
Mg	wt%	0.07	0.02	0.01	0.2	0.7	0.02	0.02
As	µg/g	118	<100	<100	<100	1356	<100	636
Mn	µg/g	<50	<50	<50	<50	204	<50	n.m.
Ni	µg/g	1261	75	80	n.m.	n.m.	40	n.m.
K	µg/g	75	155	100	<50	956	527	121
Na	µg/g	64	116	398	488	547	41	60
Al/SO_4	–	6.4	5.3	4.5	6.8	4.8	4.1	5.1

[1] Wanner et al. (2018).

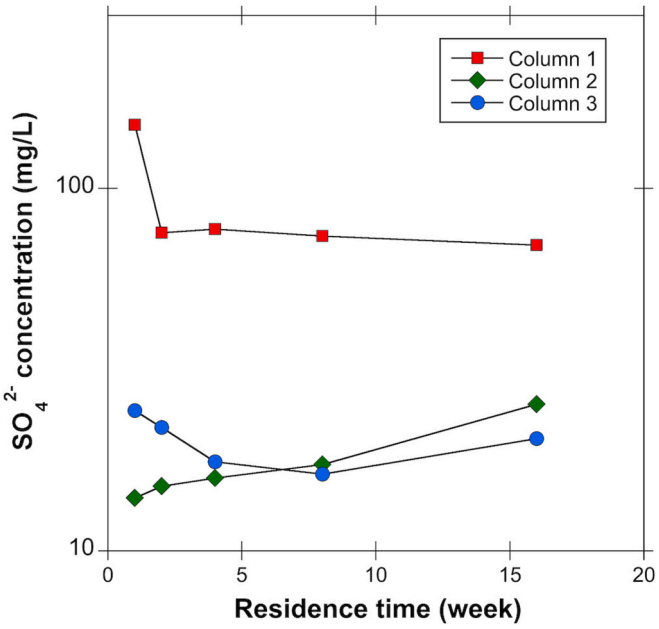

Fig. 4. Evolution of the SO_4^{2-} concentration in the effluents of the three column experiments (Table 1) as a function of the water residence time in the column. Column 1 was run with crushed rock from the Lago Vago site (0.25–2 mm), whereas Column 2 and Column 3 were run with different grain size fractions of crushed rock from the Ova Lavirun site (0.25–2 mm, 1/3 < 0.25 mm + 2/3 0.25–2 mm). The residence time refers to no flow conditions for all columns.

value at the origin of the streams (pH: 4.5–5.8, Table 2) and in the column effluent samples (5.3–6.7, Table 2). In contrast, the differences in the SO_4 and thus the total dissolved solid concentrations at the stream origins (TDS: 146–1677 mg/L, Table 2) reflect variations of the pyrite content or the subsurface residence time. As pyrite oxidation is a kinetically limited reaction (Williamson and Rimstidt, 1994), the amount of pyrite oxidation increases with increasing pyrite content and with subsurface residence time. As a result, the corresponding streamwater samples are shifted towards higher concentrations on the 1:1 correlation shown on Fig. 5. This is nicely demonstrated by the contrasting sulfate concentrations in the column experiments, which vary by a factor of about 6 (Fig. 4). The sulfur concentration of the crushed rock from the Lago Vago site (Column 1) is 5.5-fold increased in comparison to those of the crushed rocks from Ova Lavirun (Columns 2 and 3, Table 1). Since pyrite is the main sulfur source in the paragneiss rocks of the Central Eastern Alps, the difference in the pyrite content is likely on the same order of magnitude. Thus, the differences of the maximum sulfate concentrations in the column experiments (Column 1: 150 mg/L; Column 2: 25 mg/L; Column 3: 24 mg/L) almost perfectly reflect the variation of the pyrite content in the experimental material.

The decrease of the sulfate concentration with residence time initially observed for Column 1 and Column 3 (Fig. 4) likely reflects a passivation of the reactive pyrite surfaces with time. In contrast, the continuous increase of the sulfate concentration in Column 2 is a manifestation of the kinetic limitation of the pyrite oxidation reaction. Based on the much stronger sensitivity of the SO_4 concentration in the effluent with respect to the pyrite content (Table 1, Fig. 4), however, residence time variations and surface passivation appear less important for controlling the solute concentrations in ARD systems than the pyrite content. The same applies to porosity variations and hence to the water to rack ratio, although the porosity variation in our experiments (0.32–0.46, Table 1) is too small to fully assess these sensitivities. It follows that, without the presence of rock glacier ice, the pyrite content is one of the most sensitive parameters controlling the solute concentrations in aqueous solutions in contact with paragneiss rock debris.

5.1.2. The role of intact rock glaciers in accelerating weathering by sulfuric acid

Although the chemical composition of the column effluent samples is closely related to those of the streamwater samples and thus inherited from the same water-rock interaction processes, the concentrations of major solutes and toxic elements are up to two orders of magnitude lower (Table 2), even at a high residence time of 16 weeks. This implies that the formation of sulfuric acid from the oxidation of pyrite and the subsequent dissolution of aluminum and other toxic elements is strongly promoted under field site conditions where intact rock glaciers are present.

The collected streamwater samples show a very clear spatial correlation where the lowest streamwater temperatures (close to the melting point of ice), lowest pH values and highest solute concentrations always occur at the origin of the sampled streams, which is above 2600 m a.s.l. (Table 2). This demonstrates that intact rock glaciers present at the sampled stream origins (Figs. S2 and S3, Electronic Appendix) form highly efficient chemical reactors, where sulfuric acid formation and the subsequent mobilization of aluminum and other toxics elements take place. Downstream of the intact rock glaciers, merging tributaries originating from areas without permafrost or intact rock glaciers (Fig. S2, Electronic Appendix) and groundwater inflows cause the decrease in solute concentrations along the streams as discussed in detail for the Ova Lavirun system (Wanner et al., 2018).

There are several possible reasons why in the Central Eastern Alps intact rock glaciers form such strong chemical reactors. First, rock

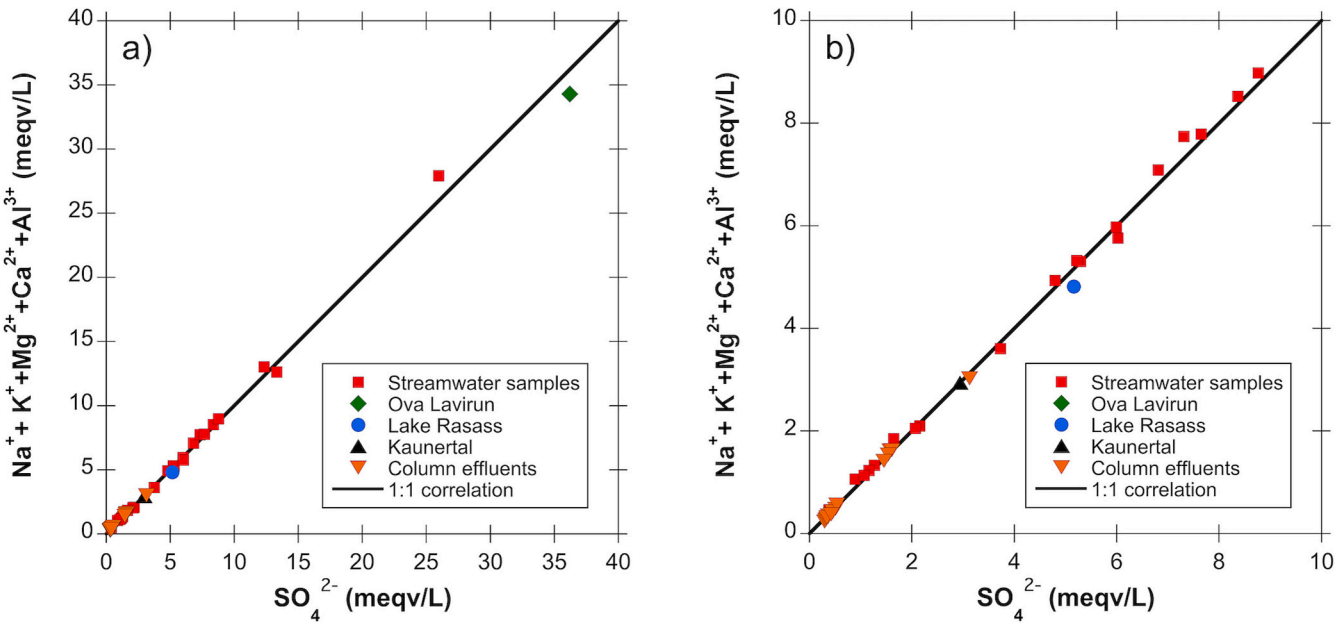

Fig. 5. a) Sum of the equivalents of major cations in the collected streamwater samples (Table 1) vs. SO_4^{2-} concentrations assuming that Al is mainly dissolved as Al^{3+} under the prevailing acidic conditions. The 1:1 correlation indicates that sulfuric acid ($H_2SO_4 \rightarrow 2H^+ + SO_4^{2-}$) is the only weathering agent in the system. Previously published analyses of streamwater samples from similar settings in the Central Eastern Alps such as Ova Lavirun (Wanner et al., 2018), the outlet of lake Rasass (Ilyashuk et al., 2018), and the outlet of the Krummgampen rock glacier in the Kaunertal (Thies et al., 2013), as well as column experiment effluent samples are plotted too. b) Insert emphasizing that the same correlation also applies at low concentrations.

glaciers operate as aquifers at high altitude allowing for sufficient interaction time to overcome the kinetic limitations of the pyrite oxidation reaction. Based on conceptual hydrogeological models of rock glaciers (Jones et al., 2019; and references therein) subsurface flow occurs as (i) supra-permafrost flow located at the top of the frozen core with very fast flow velocities of several tens to hundreds of metres per hour, and (ii) sub-permafrost flow occurring below the frozen core within a fine-grained, unfrozen base layer (Wagner et al., 2020a). The sub-permafrost base flow is rather variable and characterized by low discharge rates and subsurface water residence times on the order of days to months. Based on this model, significant pyrite oxidation occurs mainly in the fine-grained base layer where the residence time and mineral surface areas are high.

Second, compared to the rock specimen used to run the column experiments, pyrite may be enriched in the fine-grained portion of the unconsolidated rock glacier debris. Such enrichment is potentially caused by the slow creep of rock glaciers, promoting physical weathering and sorting of the different grain size fractions (Haeberli et al., 2006). Moreover, physical weathering also increases the reactive surface area of mineral grains. Both effects, pyrite enrichment as well as higher reactive surface areas, accelerate the pyrite oxidation reaction as discussed above for the column experiments. Therefore, they may contribute to the strong reactivity of the studied rock glaciers.

Third, it has been demonstrated that solutes are sequestered in permafrost (Colombo et al., 2018, and references therein) and that toxic elements such as Mn, Ni, Zn, Co can be enriched in frozen rock glacier cores. For instance, in the drillcore obtained from the Ultental rock glacier also located in the Australpine basement nappes (Northern Italy), Mn, Ni, Zn, and Co concentrations of up to 0.5, 0.4, 0.3, and 0.2 mg/L were observed in the solid ice of the drillcore (Krainer et al., 2015a). The reported enrichment demonstrates that the rock glacier ice may serve as an interim storage for elements mobilized by ARD. Partial melting of the frozen rock glacier cores in summer may thus lead to a quick and focused mobilization of these temporally stored and enriched elements.

While intact and relict rock glaciers both operate as high-alpine aquifers (Wagner et al., 2020a) and both contain fine-grained debris with possible pyrite enrichment, the temporal storage of toxic elements requires the presence of ice and is thus only possible in intact rock glaciers. Accordingly, among the three hypotheses described above, the enrichment in rock glacier ice is most likely the key for the strong mobilization of toxic elements from intact rock glaciers currently observed in the Central Eastern Alps. At present, we do not have a process-based, fundamental understanding of how the coupling between pyrite oxidation, dissolution of toxic elements and their storage in rock glacier ice actually works. Nevertheless, we hypothesize that it is only active if the temperature within the rock glacier is temporally above 0 °C. This is because pyrite oxidation and dissolution of toxic elements require the presence of liquid water at the interface between the rock glacier ice and the rock glacier debris. In-situ measurements in rock glaciers demonstrate that the temperature at the top of the frozen core may be seasonally above 0 °C (e.g. Krainer et al., 2015b). Thus, toxic element mobilization as well as their storage must occur towards the top of the frozen rock glacier core and/or in the active layer above. Based on the blocky nature and low surface area of the active layer, however, the latter is less likely. More research is required to conclusively identify, in which part of rock glaciers the sequence of coupled processes is most active and how much time for the enrichment of toxic elements in the rock glacier ice is needed to cause the high solute concentrations currently observed in the studied rock glacier springs.

5.2. Formation and fate of basaluminite

The frequent identification of basaluminite demonstrates that its formation operates as a visual manifestation for ARD occurring in permafrost or rock glacier bodies of the Central Eastern Alps. To assess the fate of aluminum in these systems, the ion activity product, *IAP*, of basaluminite was calculated using PHREEQC (Parkhurst and Appelo, 2013) in combination with the Wateq4f database assuming an ideal stoichiometry of $Al_4(OH)_{10}(SO_4)$ x 3 H_2O:

$$log(IAP) = 4\, log(a_{Al3+}) + log(a_{SO4}) + 10\, pH \quad (3)$$

Wanner et al. (2018) have shown that basaluminite precipitation in mountainous streams affected by ARD occurs almost instantaneously and exerts a strong solubility control on dissolved Al concentrations.

Therefore, the computed *IAPs* are very close the basaluminite equilibrium constant (log(*K*)) at the given sampling temperature (Wanner et al., 2018). Fig. 6 shows that the *IAPs* of basaluminite in most streamwaters from whitened stream sections (red square symbols) plot on a curve that can be well fitted by the van't Hoff relationship (Van't Hoff, 1884), typically used to describe the temperature dependence of equilibrium constants:

$$log(K)_T = log(K)_{298} - \frac{\Delta_r H^\circ}{2.303 \times R} \times \left(\frac{1}{T} - \frac{1}{298}\right) \quad (4)$$

In eq. (4), K_{298} refers to the equilibrium constant at 25 °C, $\Delta_r H^\circ$ is the standard molar enthalpy of reaction (J mol $^{-1}$), T is the temperature given in K, and *R* refers to the ideal gas constant (8.3143 J K^{-1} mol $^{-1}$). The interpolating curve (Fig. 6) thus describes the field-derived, temperature dependent equilibrium constant of basaluminite. It follows that, if the pH is constant, the solubility of basaluminite decreases with increasing temperature. Since $\Delta_r H^\circ$ was used as the fitting parameter for interpolating the log(*IAP*) values, the resulting curve allows estimating the standard molar reaction enthalpy, yielding a value of −580 kJ mol $^{-1}$, consistent with our previous estimate of −539 kJ mol $^{-1}$ (Wanner et al., 2018).

All streamwater samples from the origin of the streams (green triangles) plot below the derived solubility curve (Fig. 6). This demonstrates that these samples are undersaturated with respect to basaluminite and that the high Al concentrations (Table 2) are not solubility-controlled by the formation of basaluminite. This is consistent with the absence of basaluminite precipitates at the stream origins. Some of the stream origins, however, plot only slightly below the inferred basaluminite solubility curve (Fig. 6). This implies that, owing to the strong temperature- and *pH*-dependence of the solubility of basaluminite (Wanner et al., 2018), a minor increase in pH and/or temperature along the flow path of the streams (Fig. S2, Electronic Appendix) is sufficient to cause supersaturation and formation of basaluminite. This explains why the onset of basaluminite formation along the sampled streams occurs rather diffuse and is not necessarily triggered by a strongly neutralizing tributary such as described for the Ova Lavirun system (Wanner et al., 2018).

Three streamwater samples collected along white stream sections do not plot along the inferred solubility curve (blue circles, Fig. 6). These samples are undersaturated with respect to basaluminite, indicating that basaluminite was not forming during sampling. This confirms that streamwater compositions downstream of intact rock glaciers are seasonally variable (e.g. Brighenti et al., 2021) and that the precipitation of basaluminite at a given location may occur only temporarily.

Seasonal variations of the streamwater composition including pH may affect the stability of basaluminite and promote the alteration of previously formed precipitates. Chemical analyses of our basaluminite samples yielded a linear correlation between the Al/SO_4 ratio and the streamwater pH measured during sampling (Fig. 7). Since basaluminite serves as a strong anion-exchanger (Carrero et al., 2017b; Wanner et al., 2018), the correlation is caused by a continuous substitution reaction where one sulfate anion is replaced by two hydroxide ions, which is favored with increasing pH due to the subsequent increase in hydroxide activity. Based on other studies showing that the alteration of basaluminite with time and elevated pH is highly relevant (Lozano et al., 2018; Acero and Hudson-Edwards, 2022), the observed correlation is likely caused by an alteration of previously formed basaluminite and not by a strong variation of the formation pH of the different basaluminite samples. More research is required to study the detailed aging mechanism and fate of initially sorbed toxic elements. For the studied systems in the Central Eastern Alps such alteration, however, currently does not cause additional hazards because the mobilization of arsenic from intact rock glaciers is limited (Table S2, Electronic Appendix) and other contaminants are not enriched in the sampled basaluminite precipitates (Table 3).

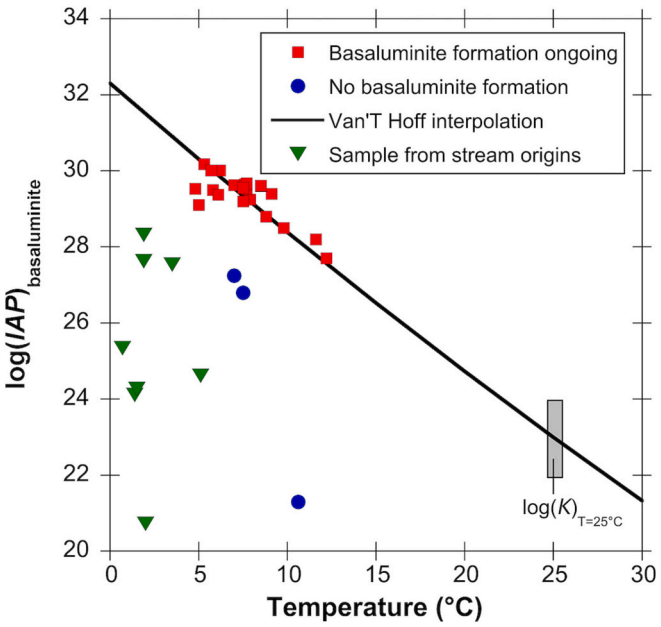

Fig. 6. Ion activity product of basaluminite (log(*IAP*)) calculated using PHREEQC for streamwater samples collected in this study (Table 2) and reported previously for the Ova Lavirun system (Wanner et al., 2018). Green triangles represent samples collected at the origin of the streams where no precipitates are forming. Blue circles and red squares denote samples collected along white-colored stream sections (Table 2). The grey rectangular illustrates the range of the basaluminite equilibrium constant (log(*K*)) reported in the literature at 25 °C (Singh and Brydon, 1969; Adams and Rawajfih, 1977; Sánchez-España et al., 2011; Lozano et al., 2018). Samples plotted as red squares are nicely matched by the van't Hoff equation (Eq. 4) when setting the reaction enthalpy ($\Delta_r H^\circ$) of basaluminite to −580 kJ/mol and the corresponding equilibrium constant to the average value reported in the literature ($\log(K)_{25^\circ C} = 23$). For these samples, precipitation of basaluminite was likely ongoing during sampling as the interpolating curve reflects the solubility of basaluminite. In contrast, samples shown as blue circle do not fall on the correlation, implying that basaluminite formation was not ongoing during sampling. (For interpretation of the references to colour in this figure legend, the reader is referred to the web version of this article.)

5.3. *Future evolution of the composition of high-alpine streams affected by ARD*

Since the formation of basaluminite represents a visual manifestation for ARD, aerial photographs can be used to qualitatively reconstruct natural ARD in high-alpine catchments over the past few decades (Zarroca et al., 2021). For the Val Costainas systems, aerial photographs only show evidence for the presence of basaluminite since the Year 2000 (Fig. 8). The onset of basaluminite formation at this time is consistent with reports of a local farmer who did not observe any precipitates in the 1990ies. In addition, similar observations were made at the Schlandraun site, where the intensity of the white-coloring of the streambed strongly increased since 2003 (Fig. S5, Electronic Appendix). It follows that the concentrations of Al and other toxic elements such as Ni, Mn, and F in the high-alpine streams affected by ARD in the Central Eastern Alps have strongly increased over the past two decades. In analogy to the Pyrenees (Zarroca et al., 2021), also in the Central Eastern Alps ARD thus serves as an indirect manifestation of climate change.

The intensification of ARD observed in the Central Eastern Alps over the past 20 years implies that the fluxes of toxic elements mobilized from rock glaciers may further increase with ongoing climate warming in the Alps (Haeberli and Beniston, 1998; Haeberli and Hohmann, 2008). If the interim storage of toxic elements in the frozen rock glacier core as postulated above is the main reason for the high concentrations of toxic elements in the affected streams, their fluxes will increase with an

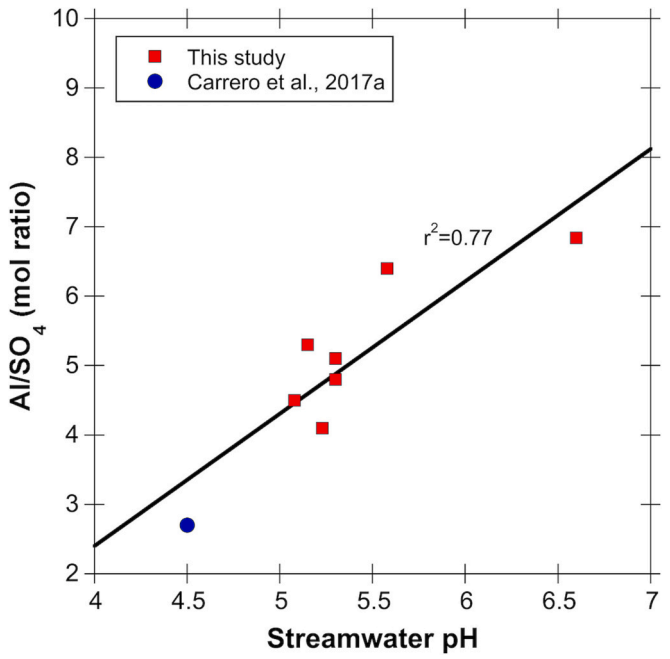

Fig. 7. Molar Al/SO_4 ratio in precipitates collected from high-alpine streams in the Central Eastern Alps (Table 1) plotted as a function of the streamwater pH measured during sampling. For comparison, the synthetic sample described by Carrero et al. (2017a) is shown as well.

accelerated melting of the frozen cores. In addition, more pyrite surfaces will be exposed to aerobic water with the ongoing rock glacier degradation, increasing the potential for sulfuric acid formation in rock glaciers. On the other hand, the water flux through rock glaciers as well as their storage capacity will likely increase (Rogger et al., 2017; Jones et al., 2019). Since groundwater in rock glacier bodies originates to a large portion from rainwater and snowmelt with low solute concentrations (Munroe and Handwerger, 2023), this will dilute the concentrations of toxic elements in the rock glacier springs. Likewise, high water fluxes in rock glaciers may decrease the subsurface residence time and hence pyrite oxidation rates. In addition, fresh pyrite surfaces that will become exposed to aerobic waters will be passivated by the formation of secondary Fe-hydroxides (Eq. (1)), also reducing pyrite oxidation rates.

Overall, the future intensity of ARD in rock glaciers is controlled by a complex coupling between climate change, ice melt, water flux, and pyrite surfaces, which is not fully understood yet. Nevertheless, we hypothesize that the flux of toxic elements mobilized from rock glacier bodies will increase in the future. A maximum will likely be reached when the degradation of intact rock glacier reaches maximum values. Because of the limited quantitative understanding of the coupled processes, however, it is currently impossible to estimate when the peak will be reached and by how much the toxic element fluxes will increase. Thus, to assess the future hazard, the water quality in the affected streams must be carefully monitored. In addition, more research is required to assess the impact of ARD on high-alpine ecosystems worldwide. Owing to the widespread occurrence of Austroalpine basement nappes (Fig. 1) and the high number of rock glaciers (5769 in Austria; 1467 in Southern Tyrol, Italy; Wagner et al., 2020b), the Central Eastern Alps are particularly affected by the identified hazard. Based on the large number of intact rock glaciers worldwide (n = ca. 40,000; Jones et al., 2018b), other regions such as South America ($n = 16{,}118$), Asia ($n = 9778$) and North America ($n = 7874$) are potentially affected as well.

6. Conclusions

The detailed investigation of six high-alpine streams affected by naturally occurring acid rock drainage in the Central Eastern Alps provided novel insights into the processes causing the mobilization of aluminum and other toxic elements from permafrost areas as well as the governing processes controlling the precipitation and stability of Al-hydroxysulfates, which serve as an important natural sink for aluminum and other toxic elements. The main conclusions and implications for the future hazard caused by ARD in intact rock glaciers in the context of global warming are listed as follows:

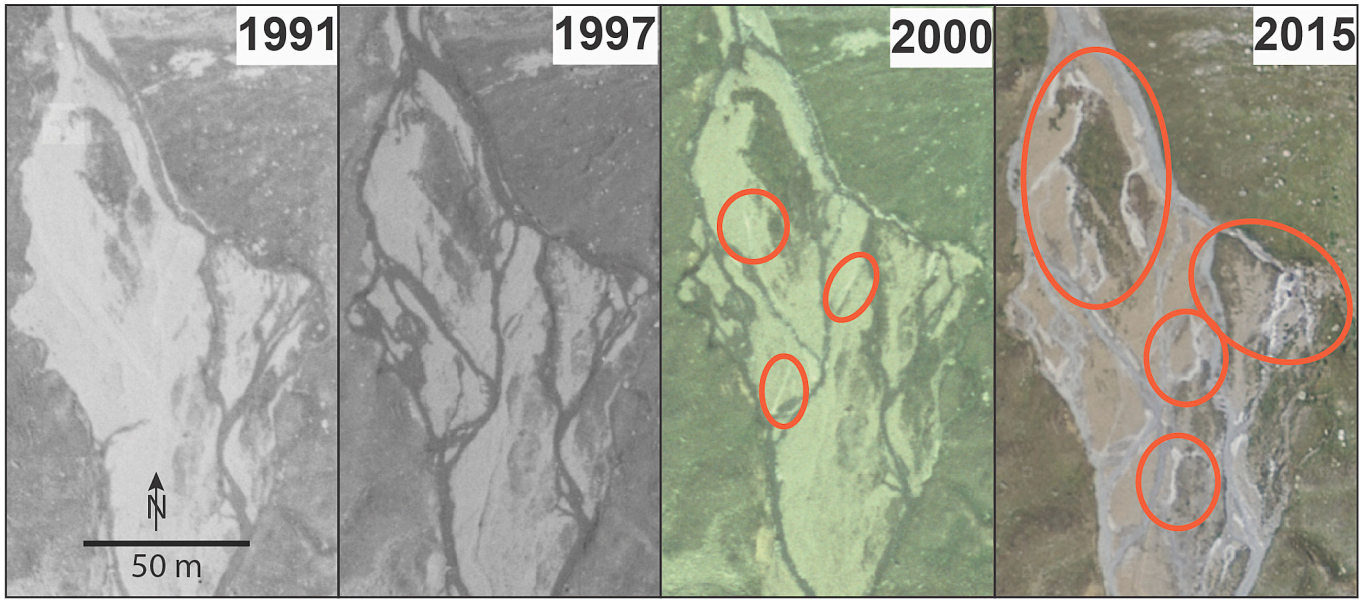

Fig. 8. Aerial pictures from Val Costainas taken in 1991, 1997, 2000, and 2015 at sampling location AP8 (Fig. S2, Electronic Appendix). The pictures are publicly available at map.geo.admin.ch. The red ellipsoids highlight stream segments, where the formation of basaluminite is clearly visible. (For interpretation of the references to colour in this figure legend, the reader is referred to the web version of this article.)

- The large number of high-alpine streams in the Central Eastern Alps affected by ARD is caused by the frequent occurrence of both, pyrite-bearing paragneisses typical for the Austroalpine basement nappes and intact rock glaciers consisting of such host rocks. Intact rock glaciers may act as highly efficient chemical reactors, resulting in high concentrations of toxic elements such as aluminum, nickel, manganese, and fluorine in the sampled streams. The most likely reason for the strong mobilization of these elements is their temporal storage and enrichment in the frozen rock glacier core, leading to a quick and focused export in summer when ice melt production rates are high.
- The precipitation of basaluminite ($Al_4(OH)_{10}(SO_4)$ x 3 H_2O) occurs downstream of rock glaciers because of the solubility decrease of basaluminite with increasing pH and temperature observed along the streams. Analysis of streamwater samples collected from stream segments with basaluminite precipitation in combination with geochemical modeling and the van't Hoff equation allowed to quantify the inverse behavior of the basaluminite solubility with temperature. This resulted in a field-derived standard reaction enthalpy ($\Delta_r H°$) of −580 kJ/ mol. This value can be used for aqueous speciation calculations to determine the saturation state of basaluminite between 0 and 25 °C and hence at temperatures relevant for permafrost areas. So far, this was only possible for a temperature of 25 °C.
- Basaluminite formation is relevant because it serves as a visual manifestation of ARD thanks to its distinct white colour. Moreover, it controls the mobility of aluminum in high-alpine streams affected by ARD and serves as a highly efficient sink for arsenic. In contrast, basaluminite does not incorporate other toxic elements such as Ni and Mn also strongly mobilized from the investigated rock glaciers.
- After formation and if exposed to higher pH values, basaluminite is subject of a continuous anion exchange reaction where SO_4^{2-} is continuously released to the solution and substituted by OH^-. Owing to the negligible mobilization of arsenic from rock glaciers in the Central Eastern Alps, this alteration currently does not cause additional hazards.
- Aerial photographs and personal reports suggest a strong intensification of ARD in the Central Eastern Alps over the past 20 years. The future intensity of ARD in rock glaciers depend on a complex coupling between climate change, ice melt, water flux, and pyrite surfaces, which is not fully understood yet. Nevertheless, it is likely that the flux of toxic elements mobilized from rock glacier bodies will increase in the future. To assess the future environmental hazard, the water quality in the affected streams must be carefully monitored. This particularly applies to the Central Eastern Alps because of the frequent occurrence of rock glaciers as well as pyrite-bearing rocks. Due to the high abundance of pyrite-bearing rocks worldwide, however, the same applies to areas downstream of rock glaciers in other regions such as South America, Asia and North America.

Declaration of Competing Interest

The authors declare the following financial interests/personal relationships which may be considered as potential competing interests:

Christoph Wanner reports financial support was provided by Swiss National Science Foundation.

Data availability

Data will be made available on request.

Acknowledgments

We thank Christopher Pichler and Priska Bähler for their analytical support concerning chemical analyses of streamwater and basaluminite precipitates. Detailed and constructive comments by two anonymous reviewers are highly appreciated. The research was partially funded by the Swiss National Science Foundation (SNF Grant 196847 to CW).

Appendix A. Supplementary data

Supplementary data to this article can be found online at https://doi.org/10.1016/j.gloplacha.2023.104180.

References

Acero, P., Hudson-Edwards, K.A., 2022. Trace element uptake in fresh and aged aluminium oxyhydroxysulfates and hydroxides: Implications for mine drainage-affected environments. Appl. Geochem. 146, 105444.
Adams, F., Rawajfih, Z., 1977. Basaluminite and Alunite: a possible Cause of Sulfate Retention by Acid Soils. Soil Sci. Soc. Am. J. 41, 686–692.
Ball, J.W., Nordstrom, D.K., 1989. Final revised anaylyses of major and trace elements from acid mine waters in the Leviathan mine drainage basin, California and Nevada—October 1981 to October 1982. U.S. Geol. Surv. Water-Res. Invest. Rep. 89–4138 (49p).
Bigham, J.M., Nordstrom, D.K., 2000. Iron and Aluminum Hydroxysulfates from Acid Sulfate Waters. Rev. Mineral. Geochem. 40, 351–403.
Blowes, D.W., Ptacek, C.J., Jambor, J.L., 2005. The geochemistry of acidmine drainage. In: Lollar, B.S., Holland, H.D., Turkerian, K.K. (Eds.), Environmental Geochemistry. Treatise on Geochemistry, vol. 9, pp. 149–204.
Boeckli, L., Brenning, A., Gruber, S., Noetzli, J., 2012. Permafrost distribution in the European Alps: calculation and evaluation of an index map and summary statistics. Cryosphere 6, 807–820.
Brighenti, S., Tolotti, M., Bruno, M.C., Wharton, G., Pusch, M.T., Bertoldi, W., 2019. Ecosystem shifts in Alpine streams under glacier retreat and rock glacier thaw: a review. Sci. Total Environ. 675, 542–559.
Brighenti, S., Engel, M., Tolotti, M., Bruno, M.C., Wharton, G., Comiti, F., Tirler, W., Cerasino, L., Bertoldi, W., 2021. Contrasting physical and chemical conditions of two rock glacier springs. Hydrol. Process. 35, e14159.
Caraballo, M.A., Wanty, R.B., Verplanck, P.L., Navarro-Valdivia, L., Ayora, C., Hochella, M.F., 2019. Aluminum mobility in mildly acidic mine drainage: Interactions between hydrobasaluminite, silica and trace metals from the nano to the meso-scale. Chem. Geol. 519, 1–10.
Carrero, S., Pérez-López, R., Fernandez-Martinez, A., Cruz-Hernández, P., Ayora, C., Poulain, A., 2015. The potential role of aluminium hydroxysulphates in the removal of contaminants in acid mine drainage. Chem. Geol. 417, 414–423.
Carrero, S., Fernandez-Martinez, A., Perez-Lopez, R., Lee, D., Aquilanti, G., Poulain, A., Lozano, A., Nieto, J.M., 2017a. The nanocrystalline structure of basaluminite, an aluminum hydroxide sulfate from acid mine drainage. Am. Mineral. 102, 2381–2389.
Carrero, S., Fernandez-Martinez, A., Pérez-López, R., Poulain, A., Salas-Colera, E., Nieto, J.M., 2017b. Arsenate and Selenate Scavenging by Basaluminite: Insights into the Reactivity of Aluminum Phases in Acid Mine Drainage. Environ. Sci. Technol. 51, 28–37.
Colombo, N., Salerno, F., Gruber, S., Freppaz, M., Williams, M., Fratianni, S., Giardino, M., 2018. Review: Impacts of permafrost degradation on inorganic chemistry of surface fresh water. Glob. Planet. Chang. 162, 69–83.
Dold, B., Gonzalez-Toril, E., Aguilera, A., Lopez-Pamo, E., Cisternas, M.E., Bucchi, F., Amils, R., 2013. Acid rock drainage and rock weathering in antarctica: important sources for iron cycling in the Southern Ocean. Environ. Sci. Technol. 47, 6129–6136.
Fortner, S.K., Mark, B.G., McKenzie, J.M., Bury, J., Trierweiler, A., Baraer, M., Burns, P. J., Munk, L., 2011. Elevated stream trace and minor element concentrations in the foreland of receding tropical glaciers. Appl. Geochem. 26, 1792–1801.
Haeberli, W., Beniston, M., 1998. Climate change and its impacts on glaciers and permafrost in the Alps. Ambio 27, 258–265.
Haeberli, W., Hohmann, R., 2008. Climate, Glaciers and Permafrost in the Swiss Alps 2050: scenarios, consequences and recommendations. In: 9th International Conference on Permafrost, pp. 607–612. https://doi.org/10.5167/uzh-6025.
Haeberli, W., Hallet, B., Arenson, L., Elconin, R., Humlum, O., Kääb, A., Kaufmann, V., Ladanyi, B., Matsuoka, N., Springman, S., Mühll, D.V., 2006. Permafrost creep and rock glacier dynamics. Permafr. Periglac. Process. 17, 189–214.
Ilyashuk, B.P., Ilyashuk, E.A., Psenner, R., Tessadri, R., Koinig, K.A., 2014. Rock Glacier outflows May Adversely Affect Lakes: Lessons from the past and present of two Neighboring Water Bodies in a Crystalline-Rock Watershed. Environ. Sci. Technol. 48, 6192–6200.
Ilyashuk, B.P., Ilyashuk, E.A., Psenner, R., Tessadri, R., Koinig, K.A., 2018. Rock glaciers in crystalline catchments: Hidden permafrost-related threats to alpine headwater lakes. Glob. Chang. Biol. 24, 1548–1562.
Jäckli, H., 1970. Kriterien zur Klassifikation von Grundwasservorkommen. Eclogae Geol. Helv. 63 (2), 389–434.
Jones, A.M., Collins, R.N., Waite, T.D., 2011. Mineral species control of aluminum solubility in sulfate-rich acidic waters. Geochim. Cosmochim. Acta 75, 965–977.
Jones, D.B., Harrison, S., Anderson, K., Selley, H.L., Wood, J.L., Betts, R.A., 2018a. The distribution and hydrological significance of rock glaciers in the Nepalese Himalaya. Glob. Planet. Chang. 160, 123–142.
Jones, D.B., Harrison, S., Anderson, K., Betts, R.A., 2018b. Mountain rock glaciers contain globally significant water stores. Sci. Rep. 8, 2834.

Jones, D.B., Harrison, S., Anderson, K., Whalley, W.B., 2019. Rock glaciers and mountain hydrology: a review. Earth Sci. Rev. 193, 66–90.
Kenner, R., Noetzli, J., Hoelzle, M., Raetzo, H., Phillips, M., 2019. Distinguishing ice-rich and ice-poor permafrost to map ground temperatures and ground ice occurrence in the Swiss Alps. Cryosphere 13, 1925–1941.
Krainer, K., Ausserer, P., Bressan, D., Lang, K., Mair, V., Mussner, L., Nickus, U., Schmidt, V., Schiestl, E.-M., Tessadri, R., Thies, H., Tonidandel, D., 2015a. Aufbau und Dynamik ausgewählter Blockgletscher in Nord- und Südtirol. Geol. Alps 12, 75–134.
Krainer, K., Bressan, D., Dietre, B., Haas, J.N., Hajdas, I., Lang, K., Mair, V., Nickus, U., Reidl, D., Thies, H., Tonidandel, D., 2015b. A 10,300-year-old permafrost core from the active rock glacier Lazaun, southern Ötztal Alps (South Tyrol, northern Italy). Quat. Res. 83, 324–335.
Lozano, A., Fernández-Martínez, A., Ayora, C., Poulain, A., 2018. Local structure and ageing of basaluminite at different pH values and sulphate concentrations. Chem. Geol. 496, 25–33.
Mair, V., Lang, K., Tonidandel, D., Thaler, B., Alber, R., Lösch, B., Tait, D., Nickus, U., Krainer, K., Thies, H., Hirnsperger, M., Sapelza, A., Tolotti, M., 2015. Projekt Permaqua: Permafrost und seine Auswirkungen auf Wasserhaushalt und Gewässerökologie im Hochgebirge. In: Brochure of the Permaque project funded by the Interreg IV program of the European Union. http://www.permaqua.eu.
Mast, M.A., Turk, J.T., Clow, D.W., Campbell, D.H., 2011. Response of lake chemistry to changes in atmospheric deposition and climate in three high-elevation wilderness areas of Colorado. Biogeochemistry 103, 27–43.
Munroe, J.S., Handwerger, A.L., 2023. Contribution of rock glacier discharge to late summer and fall streamflow in the Uinta Mountains, Utah, USA. Hydrol. Earth Syst. Sci. 27, 543–557.
Nordstrom, D.K., Alpers, C.N., 1999. Geochemistry of acid mine waters. In: Plumlee, G. S., Logsdon, M.J. (Eds.), The Environmental Geochemistry of Mineral Deposits. Vol. 6A (G.S). Soc. Econ. Geol., Littleton, Colorado, pp. 133–160. Economic Geology.
Nordstrom, D.K., Ball, J.W., Roberson, C.E., Hanshaw, B.B., 1984. The effect of sulfate on aluminum concentrations in natural waters. II. Field occurrences and identification of aluminum hydroxysulfate precipitates. In: Geological Society of America Program Abstracts, 16, p. 611.
Parkhurst, D.L., Appelo, C.A.J., 2013. Description of input and examples for PHREEQC version 3—a computer program for speciation, batch-reaction, one-dimensional transport, and inverse geochemical calculations. In: U.S. Geological Survey Techniques and Methods Book 6, chap. A43, p. 497.
PERMOS, 2020. In: Pellet, C., Noetzli, J. (Eds.), Swiss Permafrost Bulletin 2018/2019. https://doi.org/10.13093/permos-bull-2020, 20 pp.
Peters, T., 2005. Geologischer Atlas der Schweiz (1:25000), Erläuterung Atlasblatt 118. Bundesamt für Wasser und Geologie, p. 96.
Pfiffner, O.A., 2009. Geologie der Alpen. Haupt Verlag, Bern, p. 359.
Pogliotti, P., Guglielmin, M., Cremonese, E., Morra di Cella, U., Filippa, G., Pellet, C., Hauck, C., 2015. Warming permafrost and active layer variability at Cime Bianche, Western European Alps. Cryosphere 9, 647–661.
Rogger, M., Chirico, G.B., Hausmann, H., Krainer, K., Brückl, E., Stadler, P., Blöschl, G., 2017. Impact of mountain permafrost on flow path and runoff response in a high alpine catchment. Water Resour. Res. 53, 1288–1308.
Sánchez-España, J., Yusta, I., Diez-Ercilla, M., 2011. Schwertmannite and hydrobasaluminite: a re-evaluation of their solubility and control on the iron and aluminium concentration in acidic pit lakes. Appl. Geochem. 26, 1752–1774.
Schmid, S.M., Fugenschuh, B., Kissling, E., Schuste, R., 2004. Tectonic map and overall architecture of the Alpine orogen. Eclogae Geol. Helv. 97, 93–117.
Siegesmund, S., Oriolo, S., Heinrichs, T., Basei, M.A.S., Nolte, N., Hüttenrauch, F., Schulz, B., 2018. Provenance of Austroalpine basement metasediments: tightening up early Palaeozoic connections between peri-Gondwanan domains of Central Europe and Northern Africa. Int. J. Earth Sci. 107, 2293–2315.
Singh, S.S., Brydon, J.E., 1969. Solubility of basic aluminum sulfate at equilibrium insolution and in the presence of montmorillonite. Soil Sci. 107-1, 12–16.
Thies, H., Nickus, U., Mair, V., Tessadri, R., Tait, D., Thaler, B., Psenner, R., 2007. Unexpected response of high Alpine Lake waters to climate warming. Environ. Sci. Technol. 41, 7424–7429.
Thies, H., Nickus, U., Tolotti, M., Tessadri, R., Krainer, K., 2013. Evidence of rock glacier melt impacts on water chemistry and diatoms in high mountain streams. Cold Reg. Sci. Technol. 96, 77–85.
Thies, H., Nickus, U., Tessadri, R., Tropper, P., Krainer, K., 2017. Peculiar arsenic, copper, nickel, uranium, and yttrium-rich stone coatings in a high mountain stream in the Austrian Alps. Austrian J. Earth Sci. 110 (2), 1–7. https://doi.org/10.17738/ajes.12017.10012.
Todd, A.S., Manning, A.H., Verplanck, P.L., Crouch, C., McKnight, D.M., Dunham, R., 2012. Climate-Change-Driven Deterioration of Water Quality in a Mineralized Watershed. Environ. Sci. Technol. 46, 9324–9332.
Tuffnell, S., 2017. Acid Drainage: the Global Environmental Crisis You've Never Heard Of. https://theconversation.com/acid-drainage-the-global-environmental-crisis-youve-never-heard-of-83515.
Van't Hoff, M.J.H., 1884. Etudes de dynamique chimique, 3. Recueil des Travaux Chimiques des Pays-Bas, pp. 333–336.
Wagner, T., Brodacz, A., Krainer, K., Winkler, G., 2020a. Active rock glaciers as shallow groundwater reservoirs, Austrian Alps. Grundwasser 25, 215–230.
Wagner, T., Pleschberger, R., Kainz, S., Ribis, M., Kellerer-Pirklbauer, A., Krainer, K., Philippitsch, R., Winkler, G., 2020b. The first consistent inventory of rock glaciers and their hydrological catchments of the Austrian Alps. Austrian J. Earth Sci. 113, 1–23.
Wanner, C., Pöthig, R., Carrero, S., Fernandez-Martinez, A., Jäger, C., Furrer, G., 2018. Natural occurrence of nanocrystalline Al-hydroxysulfates: Insights on formation, Al solubility control and as retention. Geochim. Cosmochim. Acta 238, 252–269.
Williamson, M.A., Rimstidt, J.D., 1994. The kinetics and electrochemical rate-determining step of aqueous pyrite oxidation. Geochim. Cosmochim. Acta 58, 5443–5454.
Zarroca, M., Roqué, C., Linares, R., Salminci, J.G., Gutiérrez, F., 2021. Natural acid rock drainage in alpine catchments: a side effect of climate warming. Sci. Total Environ. 778, 146070.